applied sciences

MDPI

Article

Zero-Dimensional Modeling of the Rate of Injection with a Diesel Common Rail System Using Single-Hole Nozzles with Neat Low-Carbon Fuels

Vicente Rojas-Reinoso [1,*], Carmen Mata [2], Jose Antonio Soriano [3] and Octavio Armas [3]

[1] Grupo de Ingeniería Automotriz, Movilidad y Transporte (GiAUTO), Carrera de Ingeniería Automotriz-Campus Sur, Universidad Politécnica Salesiana, Quito 170702, Ecuador
[2] Escuela de Ingeniería Minera e Industrial de Almadén, Instituto de Investigación Aplicada a la Industria Aeronáutica, Campus de Excelencia Internacional en Energía y Medioambiente, Universidad de Castilla-La Mancha, 13400 Almadén, Spain; mariacarmen.mata@uclm.es
[3] Escuela de Ingeniería Industrial y Aeroespacial, Instituto de Investigación Aplicada a la Industria Aeronáutica, Campus de Excelencia Internacional en Energía y Medioambiente, Universidad de Castilla-La Mancha, Av. Carlos III s/n Castilla-La Mancha, 45071 Toledo, Spain; joseantonio.soriano@uclm.es (J.A.S.); octavio.armas@uclm.es (O.A.)
* Correspondence: erojas@ups.edu.ec

Abstract: This paper presents a fuel injection rate predictive model based on zero-dimensional correlations from experimental results. This model estimates the fuel injection rate behavior with varying parameters such as fuel injection pressure-injector energizing, the injection nozzle geometrical characteristics, and fuel viscosity. The model approach was carried out with diesel fuel. Then, the model was applied to the use of two alternative low-carbon fuels without diesel. An experimental methodology was used under controlled conditions, employing an injection rate indicator to measure the injection parameters in real time. The setup was carried out on a pump test bench using a common rail injection system. The results show that the model can be adapted to different injection conditions and fuels.

Keywords: diesel injection; solenoid-operated; fuel injection rate modelling; zero-dimensional model; GTL fuel; HVO fuel; fuel injection pressures

Citation: Rojas-Reinoso, V.; Mata, C.; Soriano, J.A.; Armas, O. Zero-Dimensional Modeling of the Rate of Injection with a Diesel Common Rail System Using Single-Hole Nozzles with Neat Low-Carbon Fuels. *Appl. Sci.* **2024**, *14*, 2446. https://doi.org/10.3390/app14062446

Academic Editors: Jun Cong Ge and Krzysztof Biernat

Received: 26 January 2024
Revised: 28 February 2024
Accepted: 11 March 2024
Published: 14 March 2024

1. Introduction

In the last 30 years, strict government policies have been developed to restrict the emission levels of pollutants that mainly affect the emission of nitrogen oxides (NOxs), carbon monoxide (CO), hydrocarbons (HCs), and particulate matter (PM). Implementing these environmental policies is also intended to reduce the consumption of fossil fuels and encourage the use of alternative low carbon fuels, such as biodiesel, gas-to-liquid, hydrotreated vegetable oil, and farnesane, which also contribute to reducing pollutant emissions.

Manufacturers of fuel injection systems develop these systems focusing on the improvement of the combustion process for reducing pollutant emissions according to the requirements of environmental regulations, increasing their efficiency and, therefore, the brake engine efficiency. Numerous researchers have shown that fuel injection parameters significantly impact pollutant emissions [1–4]. Research on the efficiency of injection systems focuses on improving fuel atomization and optimizing the injection process to achieve the best possible combustion in the cylinder. The rate of fuel injection (RoI) is closely related to the heat release rate of the fuel; therefore, analyzing the parameters that directly or indirectly affect the injection rate makes it possible to know how the fuel heat will be released during the combustion process.

Alternative fuels are one of the most promising ways to reduce pollutant emissions, along with modern catalytic aftertreatment systems [5–10]. Traditional biodiesels have been

a promising substitute for diesel because of their good thermal efficiency and low CO and SOx emissions [8]. However, other aspects related to crop and food availability have led to the search for alternative fuels, including third-generation synthetic fuels such as farnesane or hydrotreated vegetable oil (HVO). These synthetic fuels have high thermal efficiency and lower emissions than traditional biodiesel [11–14]. The influence of biodiesel properties on injection parameters has been extensively studied in traditional biodiesels [2,3,15–17], although it has been studied to a lesser extent on these synthetic fuels [18–20].

Varying injection parameters such as injection timing, injection pressure, and fuel spray duration is one of the strategies to improve engine performance [2,21–24] that can be combined with the use of alternative fuels to reduce emissions. In injection systems, the fuel injection rate depends on different control variables, such as injector nozzle geometry and injector type, engine load, properties of the fuel used, and injection characteristics (multiple injections, injection pressure, injection duration, etc.) [25–28]. This large variability of study parameters complicates experimentation. Most researchers use robust test benches and fuel injection rate indicator equipment [29] to reproduce the operating situations of injection systems in vehicles. However, these facilities are costly and complex to maintain, making it difficult for universities or companies with fewer resources to access this type of facility.

Injection rate simulations are a valuable tool for the reduction of experimental time and error reduction, allowing the simulation of operating conditions that would be dangerous for the experimental equipment. Simulations of injection rates can be performed with zero-dimensional (0D) models [30,31], or multidimensional models in combination with other mathematical and software tools [32–34]. 0D models are simple to implement and require limited experimental trials [29].

In 0D models, the injection time variation is the most commonly used parameter for studies focused on combustion behavior, emissions, and fuel consumption [29]. Although other injection parameters, such as injection pressure, injector energizing time [29,35–37], or injector nozzle geometry [38,39] have also been varied.

Regarding the injector geometry, some studies have reported the influence of the number of holes in the cavitation processes with different fuels [40,41], and recommended a study with single-hole nozzles to know the behavior of the injection rate more deeply. The variation of nozzle diameters provides valuable information on how geometrical factors can influence the injection rate and ultimately affect the performance and efficiency of the fuel injection system.

Although 0D models for injection rate are simple, they are less commonly used compared to one-dimensional (1D) models [29]. Payri R. et al. [42] developed a 0D model capable of estimating the shape of the injection rate and the amount of fuel mass injected with the lowest possible computational cost. In this work, the rate curve is divided into three parts, and mathematical expressions of straight slopes are used to open and close the fuel injection rate curve, which combines second-order Bézier curves to smooth the corners. Xu et al. [43] divided the injection process into five stages and used different mathematical strategies to model each stage, even combining the data from other experimental works, such as those of Agarwal et al. [44], Seykens et al. [45], and Li et al. [46]. In Soriano et al. [31], a model is presented that divides the injection rate curve into three parts: the rising phase (from the beginning of injection until it reaches the maximum value of the injector opening that coincides with the one obtained in Equation (10)), the middle phase (in which the maximum amount of fuel is injected), and the falling phase (since the amount of fuel injected begins to decrease). Gao et al. [47] developed a model using a similar methodology to Soriano et al. [31]. They used experimental correlations with parameters related to injector operation, fuel properties, and operating conditions to determine the start of injection time, the end of injection time, and the slopes of the RoI curve. Perini et al. [48] divided the rate-of-injection curve into four sections (1st needle lift, 2nd full-lift hydraulic transient, 3rd steady state max rate, and 4th descent) to develop the 0D model. The model combines the theoretical injection equations with the information obtained from the experimental tests for each section.

In this research, a 0D model is proposed to obtain the injection rate from certain operating conditions, such as injection pressure, energizing time, and fuel temperature. In addition, the geometry of the injector nozzle and some of the fuel properties are used. Injectors with single-hole nozzles were used to avoid the uncertainties caused by using multiple-hole nozzles on the rate of fuel injection. Data from two synthetic paraffinic fuels have been included so that the model can simulate the rates of these fuels and extend the usefulness of the model obtained. The model proposed in this work is based on other 0D models already published [42,43,47,48], but particularly, it is an evolution of the model presented by Soriano et al. [31]. The novelty of this article compared to previous ones lies in the way in which the phases into which the fuel injection rate is divided are established, using mathematical correlations that do not require the calculation of the phase shifts between the energizing signal and the RoI signal.

2. Materials and Methods

2.1. Experimental Installation

Figure 1 shows the experimental setup used in the present investigation, which is described in detail in Soriano et al. [31].

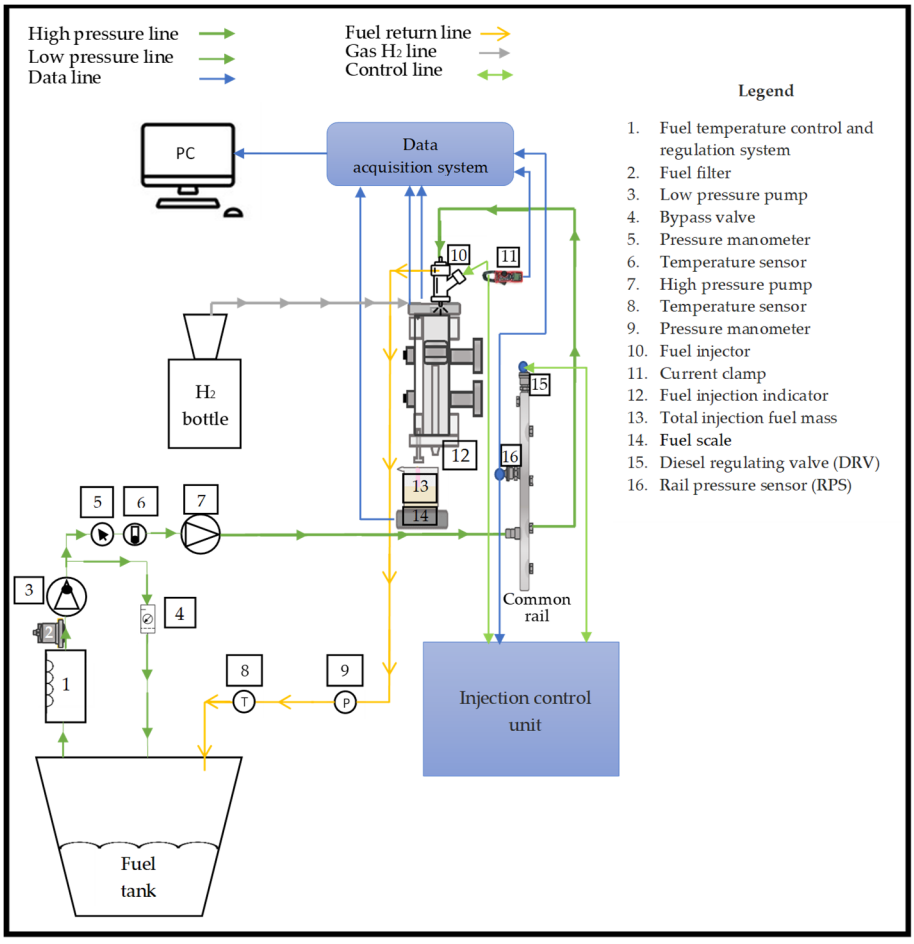

Figure 1. Functional scheme of the experimental facility.

A pump injection test bench is responsible for supplying the appropriate fuel flow to the high-pressure pump of the injection system so that it raises the pressure and sends the fuel to the rail. The pressure-regulating valve delivers the fuel from the common rail to the injector at the pressure and temperature conditions set for the test. The dyno control system controls the pump pressure, injector pulse, injection frequency and pressure, and injector injection timing.

A fuel injection indicator model EVI-2 K-050-49 (Hantek®, Qingdao, China) was used to determine the injection rate measurement experiments using the Bosch method [49]. The EVI control unit displays the static system's fuel temperature and back pressure.

The injector activation pulse was detected using a Hantek® CC 65 AC/DC current clamp with a bandwidth of 20 kHz to measure the working intensity of the pulse. The total mass of fuel injected (mf) was measured by a Kern PFB 3000-2 gravimetric balance (Balingen, Germany). All generated signals were viewed with an oscilloscope and captured by a data acquisition system (Yokogawa DL708E, Tokyo, Japan). More details about this experimental setup and the measurement methods used can be found in [31,50].

A Bosch 089909/0445110239 solenoid-type injector (Gerlingen, Germany) was used in this work. The three nozzles used have a K-factor of 3.5 and a single orifice (mono-centric). The hole diameters of the nozzles are 115, 130, and 150 µm in diameter, respectively. A Nikon CT-Scan-XT-H-160 X-ray scanner (Tokyo, Japan) was used to obtain the geometrical characteristics of the injector nozzles. This scanner generated three-dimensional (3D) images from two-dimensional (2D) images of the nozzles. In addition, image reconstruction software (VGStudio Max 2.2) was implemented to perform data evaluation to calculate variables such as areas, volumes, porosity, thickness, density, etc. Figures 2–4 show the images obtained and the dimensions of each of the nozzles used in the tests.

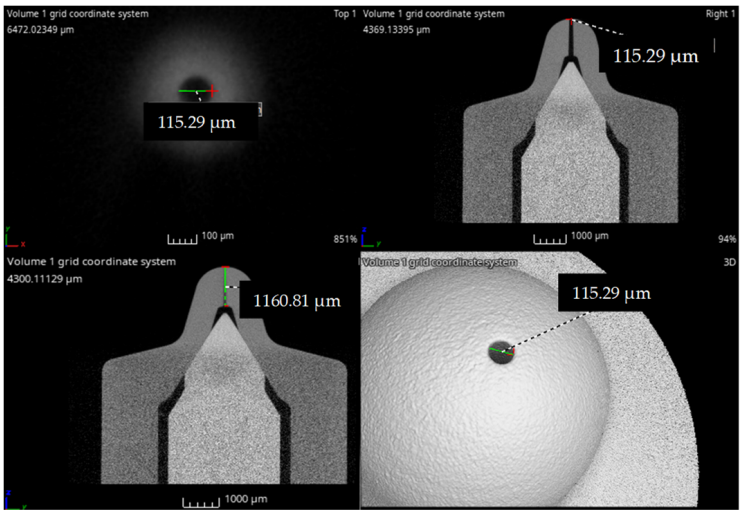

Figure 2. 115 µm nozzle X-ray.

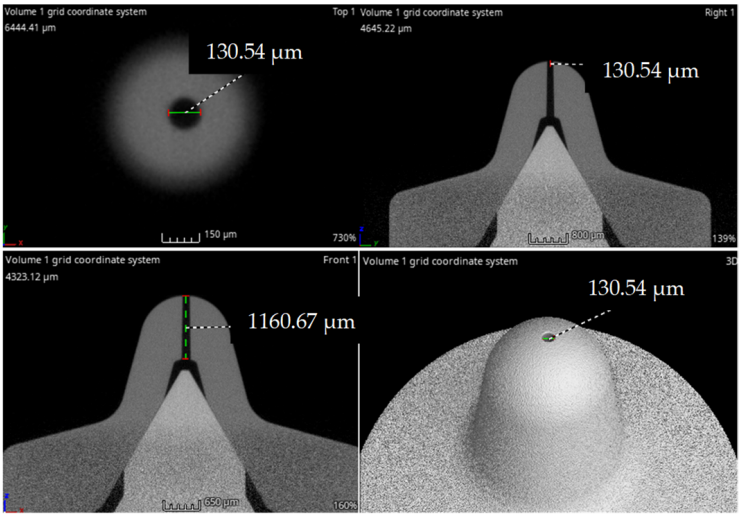

Figure 3. 130 µm nozzle X-ray.

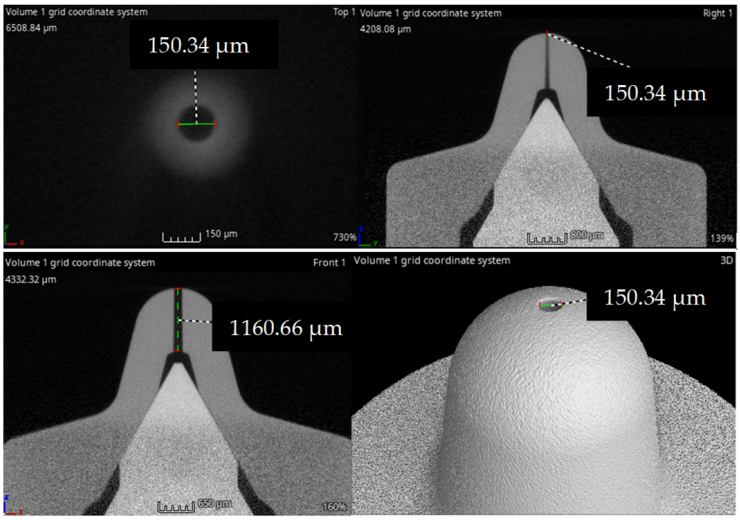

Figure 4. 150 µm nozzle X-ray.

The measurement errors associated with each component of the experimental installation are detailed in Table 1.

Table 1. Equipment errors.

Name	Error of Full Scale (%)
Diesel Regulator Valve (DRV)	±2
Temperature Sensors	±1
Current clamp	±2
Gravimetric balance	±0.01
Sensor connection wires	±0.0064
Fuel rate indicator	±0.6
Rail Pressure Sensor (RPS)	±5
Line Pressure Sensors (LPS)	±1.3

2.2. Test Fuel

2.2.1. Fuel Properties

One hydrotreated vegetable oil (HVO) fuel, supplied by REPSOL (Madrid, Spain), and one gas-to-liquid (GtL) fuel, supplied by SASOL, were used in this study, the results of which were compared with a commonly used diesel fuel (supplied by REPSOL). The fuels' characteristics are shown in Table 2.

Table 2. Fuels Properties.

Properties	Diesel	HVO	GtL
Relation H/C [a]	1.84	2.06	5.53
Stoichiometric air–fuel ratio [a]	1/14.45	1/14.71	1/14.7
C (% p/p) [b]	86.20	85.7	84.67
H (% p/p) [b]	13.80	14.3	15.31
O (% p/p) [b]	0	0	0
Density @ 15 °C (kg/m^3) [b]	845	775	773
Density @ 25 °C (kg/m^3) [b]	840	769	767
Density @ 40 °C (kg/m^3) [b]	827	761	757.5
Viscosity to 15 °C (cSt) [b]	5.24	3.99	4.66
Viscosity to 25 °C (cSt) [b]	4.64	3.41	3.91
Viscosity to 40 °C (cSt) [b]	3.55	2.57	2.97
High calorific value (MJ/kg) [b]	45.97	47.24	46.91
Low calorific value (MJ/kg) [b]	43.18	44.20	43.66

Table 2. *Cont.*

Properties	Diesel	HVO	GtL
Cold filter plugging point (°C) [b]	−19	−40	−45
Lubricity (WS1.4) (μm) [b]	237	334	548
Cetane number [b]	54.2	94.8	71
Flashpoint (°C) [b]	61	70	63
Distillation (vol) [b]			
10% (°C)	206.5	265.2	195
50% (°C)	275.9	278.5	260
90% (°C)	344.9	290.4	338

The prefixes "[a]" and "[b]" mean calculated and measured, respectively.

2.2.2. Fuel Density Estimation

When pressure and temperature conditions are modified, the fuel density also undergoes changes, which impacts the accuracy and stability of the injection rate. To address this aspect, Equation (1) is used for diesel fuel obtained according to the methodology presented by Payri et al. [51].

$$\rho_{Diesel}(P,T) = 835,698 - 0.628(T-T_0) + 0.491(P-P_0) - 0.00070499(T-T_0)^2 + 0.00073739(P-P_0)^2 + 0.00103633(P-P_0)(T-T_0) \quad (1)$$

In all equations in this section, P_0 and T_0 refer to the set pressure and temperature conditions.

Equations (2)–(4) for GtL fuel were obtained according to the methodology presented by Outcalt [52]. Equation $\rho(P_0,T)$ is calculated from the equation proposed by Rackett [53] and the experimental data in Table 1, and where $B(T)$ is the Tait equation parameter defined by Dymond et al. [54], valid for any fuel with the characteristics of GtL and HVO fuel. Equations (1)–(4) were used by Soriano et al. [31] for the development of their model.

$$\rho(P,T) = \frac{\rho(P_0,T)}{1 - 0.082681 \cdot \ln\left(\frac{P+B(T)}{P_0+B(T)}\right)} \quad (2)$$

$$\rho_{GTL}(P_0,T) = 255.5 \cdot 0.519^{-(1+(1-T/578.2)^{0.542})} \quad (3)$$

$$B(T) = 325.49 - 298.96T/273 + 70.73(T/273)^2 \quad (4)$$

For the calculation of the density variation equation with pressure and temperature of the HVO fuel, the same methodology is used as for the GtL fuel, using Equations (2), (4), and (5).

$$\rho_{HVO}(P_0,T) = 257.1 \times 0.518^{-(1+(1-\frac{T}{578.1})^{0.55})} \quad (5)$$

2.2.3. Fuel Dynamic Viscosity Estimation

To determine the equations that determine the behavior of viscosity with temperature, we use the equations presented by Soriano et al. [29] for diesel fuel (Equation (6)) and GtL (Equation (7)).

$$\mu_{Diesel}(P_0,T) = 5.7694e^{-0.0169T} \quad (6)$$

$$\mu_{GTL}(P_0,T) = 4.788e^{-0.0189T} \quad (7)$$

In the case of HVO, an exponential expression (Equation (8)) obtained from the experimental data shown in Table 1 is used.

$$\mu_{HVO}(P_0,T) = 4.1061e^{-0.018T} \quad (8)$$

In these three expressions, the kinematic viscosity is given in cPo, and the fuel temperature is given in °C. To know the variation of viscosity with pressure, Equation (9), proposed by Kousel, is used [55].

$$\mu_f(P,T) = \mu_f(P_0,T)exp\left[\frac{P}{10^4}\left(7.9718 + 37.27967\mu_f(P_0,T)^{0.278}\right)\right] \quad (9)$$

In this work, kinematic viscosity (v_f) has been used instead of dynamic viscosity because the former indirectly includes the density value, which allows using one less parameter for the development of correlations.

2.3. Test Plan

In the present work, a solenoid injector with three different single-bore nozzles with diameters of 115 µm, 130 µm, and 150 µm, respectively, was used. To develop the tests, 3 energizing times (ET), 4 injection pressures (P_{inj}), and 2 fuel temperatures (T_f) were established. The back pressure in the rate of injection indicator was set at 5 MPa for all tests. Fuel temperature was measured at the inlet of the high-pressure pump. Tests were conducted with two fuel temperatures at the inlet of the high-pressure pump to study the effect of fuel temperature at the inlet.

The experimental test plan developed with each fuel is shown in Table 3. Each of the tests was repeated 5 times, presenting as results in all tests, the average of these 5 experiments.

Table 3. Test plan.

P_{inj} (MPa)	ET (ms)	T_f (°C)
50/70/90/110	1	20
		40
	1.5	20
		40
	2	20
		40

After performing the experimental tests, the 54 tests from which the model will be obtained are selected. These tests correspond to all those carried out at pressures of 90 and 110 MPa with the three fuels and the three nozzles.

The range of injection pressures tested covers the possible test conditions allowed by the fuel injection system used. However, the values of 50 and 70 MPa are those values where the measured fuel injection rate has more irregularities compared to other higher injection pressure values (90 and 110 MPa). Part of these experimental data were used for model implementation. Different data were used for model validation.

The data required for the development include all the variables that define each test (fuel properties and temperature, orifice diameter, injection pressure, energizing time) as input data of the model. Some variables obtained from the tests, such as the time from the beginning of energizing to the end of the injection rate (hereafter, d_0) and the mass injected during the injection event, were used as output of the model.

2.4. Model Proposed Methodology

Theoretically the calculation of the mass injected during fuel injection is obtained by Equation (10). However, assuming this value involves assuming that the fuel injection rate curve is a square pulse, when the rate curve usually has more of a trapezoidal or triangular shape,

$$\dot{m}_f = C_d A_0 \sqrt{2\rho_f\left(P_{inj} - P_{back}\right)} \quad (10)$$

where C_d is the discharge coefficient, A_0 is the geometric outlet section of the nozzle orifice, P_{inj} is the injection pressure, P_{back} is the back pressure, and ρ_f is the fuel density.

For this study, the ranges used for the development of the injection pressure and energizing time tests result in trapezoidal rate curves in all cases, because this model is developed only for rate simulation of this type.

Although it uses concepts developed by other authors [42,43,47,48], the model proposed is an evolution of the model presented by Soriano et al. [31]. On this occasion, the model presented divides the injection rate curve into three parts as shown in Figure 5, but now all these phases are modeled by curved lines using correlations. The three new correlations already include the lags between the energizing signal and the RoI signal, both at the beginning and at the end of the RoI.

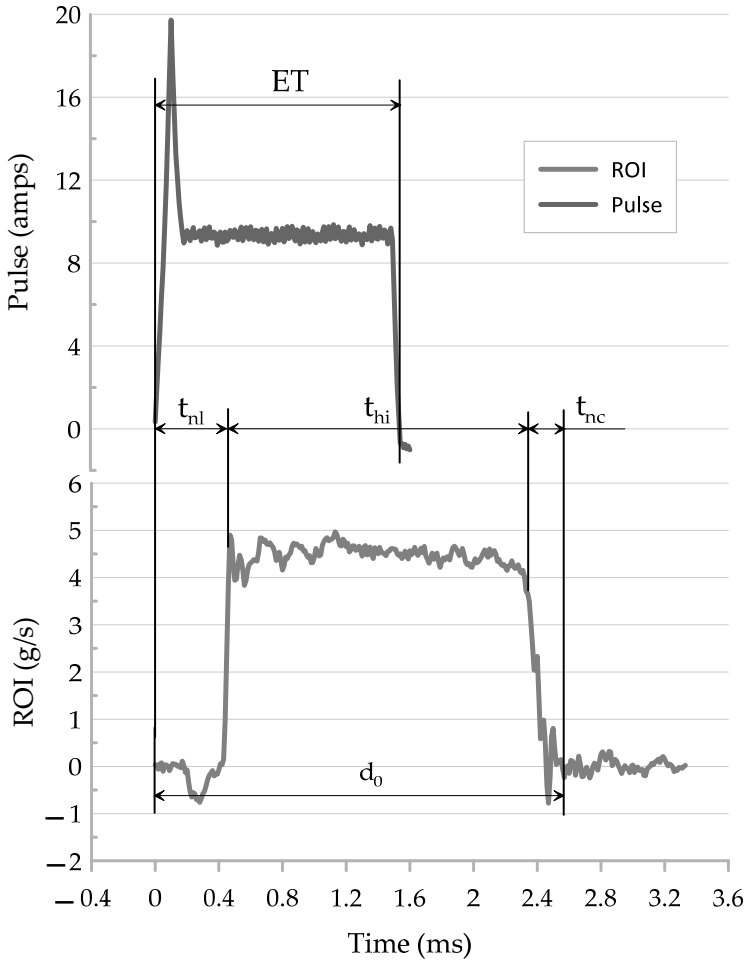

Figure 5. Real experimental event of the fuel injection process.

In this work, 3 phases are also used to generate the fuel injection rate curve (as in Soriano et al. [31]) but using a different methodology.

Figure 6 shows the variation of the injection pulse and the injected mass as a function of time for a fuel injection rate event. This figure also shows the three phases into which the fuel injection rate curve is to be divided:

- The first phase describes the time lag between the beginning of the injector energizing until the beginning of the fuel injection ramp. This time is referred to the 'needle lift' (t_{nl}), corresponding to a situation where the needle is moving to let the fuel through.
- The second phase into which the rate curve is divided describes the steady state of the rate curve. In this phase, the needle is entirely open. The time this phase occurs has been termed 'holding injection' (t_{hi}) since it corresponds to the time in which the injection rate curve is stable.
- The third phase describes the decrease in fuel flow during injector closure. This time is called 'needle closure' (t_{nc}) since it corresponds to a situation in which the needle is moving to close the fuel outlet. It must be considered that the closing process does not consider the residual injections that occur at the end of the injection process.

In addition to the time that each phase lasts, another time parameter has been defined to describe the sum of time that these three phases last, which has been called 'test time' (d_0) and which corresponds to the time from the beginning of the energizing to the end of the injection rate.

An analysis of the representativeness variables in the numerical models allows us to know these variables' dependence on the injection rate. Therefore, the first step in model development is determining the relevance of the variables used for model prediction. The variables involved in the injection process in this work are energizing time (ET) measured in ms, injection pressure (P_{inj}) measured in MPa, fuel properties (specifically, the kinematic viscosity (v_f, measured in mm^2/s), hole diameter (z) measured in µm, test time (d_0) measured in ms, and fuel temperature (T_f) measured in °C. Contrary to Soriano et al. [31], in this case, the back pressure is constant (5 MPa) as well as the number of holes (1 single hole); therefore, these are two variables that will not participate in the modeling of the rate curve. The representative variables were verified separately in each phase to improve the model's ability to reproduce the fuel injection rate curve.

Figure 6 shows the relevance of the participating variables in this study, indicating which should be included in the prediction models for each phase.

- In the case of the 'needle lift' phase, Figure 6a shows that d_0 is the most relevant factor due to the stability or low variability of the data. This fact indirectly implies that the most significant variability or dependence is due to P_{inj} and the kinematic viscosity of the fuel. Figure 6d shows that the most representative variables are P_{inj} and d_0, followed by hole diameter, fuel viscosity, and energizing time. In all cases, this is because the slope of the rate curve is similar in almost all tests.
- In the case of the 'holding injection' phase (Figure 6b), the variables of major dependence to keep the injection stable during this phase are the hole diameter and the injection pressure. Figure 6e indicates that the most representative variable is the energizing time since it generates a more noticeable change in the time the injector is open and, as such, in the duration of the injection time.
- Finally, for the 'needle closure' phase (Figure 6c), the most relevant variable is again d_0, along with energizing time. Figure 6f shows that the specific control variable in the equation is energizing time, followed directly by P_{inj} and d_0.

In summary, in all phases, the injection rate depends on test time, injection pressure, injector energizing time, nozzle bore diameter, and kinematic viscosity. However, in none of the phases is fuel temperature identified as an essential dependent variable.

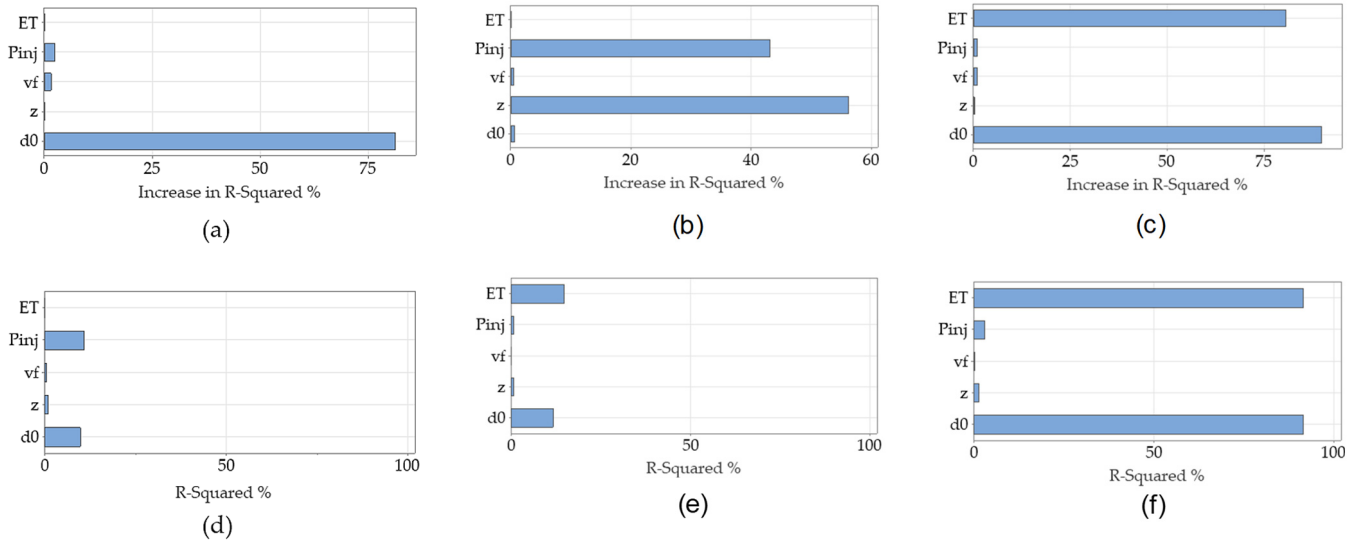

Figure 6. Description of relevance of variables of linear prediction models: (**a**,**d**) needle lift phase, (**b**,**e**) holding injection phase, and (**c**,**f**) needle closure phase.

Once the variables that provide the most remarkable dependence on the behavior of the rate in the injection process have been found, a numerical statistical model is generated that simulates the injection rate concerning the dependent variables. This model establishes a mathematical dependence correlation according to the variables involved in each phase.

The linear predictive model obtained for the 'needle lift' (phase 1) is shown in Equation (11), and the values of the coefficients are shown in Table 4.

$$t_{nl} \approx -a_1 - a_2 * ET + a_3 * P_{inj} + a_4 * v_f - a_5 * z - a_6 * d_0 - a_7 * {P_{inj}}^2 - a_8 * {v_f}^2 + a_9 * z^2 + a_{10} * {d_0}^2 + a_{11} * ET * d_0 + a_{12} * P_{inj} * d_0 - a_{13} * v_f * d_0 + a_{14} * z * d_0 \quad (11)$$

Table 4. Value of the coefficients of Equation (11).

a_1	0.98	a_8	0.842
a_2	0.0422	a_9	0.00006953.834
a_3	0.000022	a_{10}	0.1376
a_4	5.189	a_{11}	0.0088323.098
a_5	0.02297	a_{12}	0.01630
a_6	31.401	a_{13}	0.842
a_7	0.000002	a_{14}	0.00006953.834

Equation (12) provides the mathematical correlation describing the holding injection phase, and the values of the coefficients are shown in Table 5.

$$t_{hi} \approx b_1 - b_2 * ET - b_3 * P_{inj} - b_4 * v_f - b_5 * z + b_6 * d_0 + b_7 * ET^2 - b_8 * {P_{inj}}^2 + b_9 * {v_f}^2 + b_{10} * z^2 - b_{11} * {d_0}^2 + b_{12} * ET * P_{inj} + b_{13} * ET * v_f - b_{14} * ET * z + b_{15} * ET * d_0 + b_{16} * P_{inj} * v_f + b_{17} * P_{inj} * z - b_{18} * P_{inj} * d_0 + b_{19} * v_f * z + b_{20} * v_f * d_0 + b_{21} * z * d_0 \quad (12)$$

Table 5. Value of the coefficients of Equation (12).

b_1	15.046	b_{12}	0.000066
b_2	0.2855	b_{13}	0.02353
b_3	0.001719	b_{14}	0.000259
b_4	9.285	b_{15}	0.10073
b_5	0.04942	b_{16}	0.000057
b_6	0.3324	b_{17}	0.000046
b_7	0.02157	b_{18}	0.000028
b_8	0.000001	b_{19}	0.003499
b_9	1.6995	b_{20}	0.01867
b_{10}	0.000183	b_{21}	0.000743
b_{11}	0.17902		

The analysis based on independent values for the needle closure phase provided the mathematical expresion shown in Equation (13), and the values of the coefficients are shown in Table 6.

$$t_{nc} \approx c_1 + c_2 * ET - c_3 * P_{inj} + c_4 * v_f - c_5 * z - c_6 * d_0 + c_7 * ET^2 + c_8 * z^2 + c_9 * {d_0}^2 - c_{10} * ET * P_{inj} + c_{11} * ET * v_f - c_{12} * ET * z - c_{13} * ET * d_0 + c_{14} * P_{inj} * d_0 - c_{15} * v_f * z - c_{16} * v_f * d_0 + c_{17} * z * d_0 \quad (13)$$

2.5. Models Accuracy

An average absolute error of 1.84%, related to the values presented in Table 1, was obtained in the evaluation process. The coefficient of determination (R^2) values were 90.02%, 97.24%, and 90.45% for the phases 'needle lift', 'holding injection', and 'needle closure', respectively. The high R^2 values indicate an excellent agreement between the experimental

data and those obtained from the presented prediction models. A confidence value of 92% was applied in each case to validate the accuracy of the proposed predictive models.

Table 6. Value of the coefficients of Equation (13).

c_1	42.452	c_{10}	0.003340
c_2	74.621	c_{11}	1.4541
c_3	0.003723	c_{12}	0.01556
c_4	1.975	c_{13}	62.628
c_5	0.02427	c_{14}	0.003203
c_6	73.444	c_{15}	0.002795
c_7	31.159	c_{16}	1.4098
c_8	0.000062	c_{17}	0.01392
c_9	31.228		

3. Results

Experimental Results

As stated in the previous section, to develop the model, it is necessary to know the injected mass of fuel. In Supplementary Materials, Table S1 shows the fuel mass values of each experimental test injected in one injection. These values have been obtained from the average of the five tests carried out for each condition established in the test plan.

As an example, Figure 7a,b represent the mean value of each of the tests performed with its confidence interval for the tests performed at a fuel temperature of 20 °C (Figure 7a) and at a temperature of 40 °C (Figure 7b) with an injection pressure of 90 MPa. It is observed that the fuel temperature in the ranges used minimally affects the fuel injection rate. At the same time, the nozzle bore size and ET are the variables that cause the most variability in the results. Logically, the larger bore-size nozzle produces a higher fuel injection rate. Regarding the fuels, in all cases, more diesel fuel is injected, followed by HVO, and finally, GtL fuel, although the difference between them is slight. This result may be because cavitation is higher with GtL [56] and HVO fuels [41].

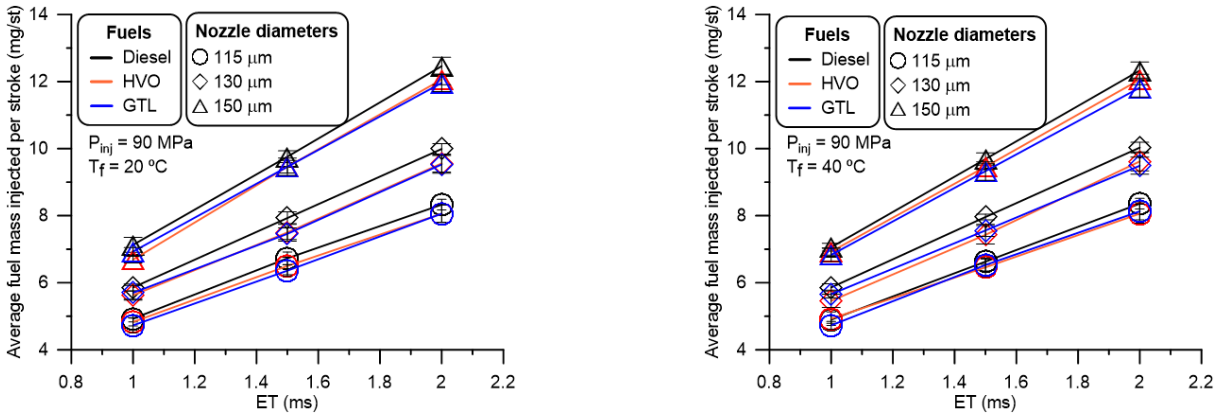

Figure 7. Behavior of the injection rate with its control parameters: (**a**) fuel temperature to 20 °C, (**b**) fuel temperature to 40 °C.

In Supplementary Materials, Tables S2–S4, show the injection timing values concerning the injector energizing of the experimental tests with every nozzle. In each cell, it is indicated at the beginning and the end of each phase in which the fuel injection rate curve has been divided, concerning the beginning of the energizing.

As an example, Figure 8a,b represent the mean value of each of the tests performed at a fuel temperature of 20 °C, with ET of 1 ms (Figure 8a) and ET of 2 ms (Figure 8b) for all fuels and all nozzles, but only for the first phase, since it is the phase that most depends on the variation of the parameters of this study. In both figures, it is observed that

the increase in pressure reduces the duration of the first phase and makes it more stable, even independent of the properties of the fuels. Figure 8a,b are similar, so the duration of energizing does not affect this first phase. Regarding the size of the hole, especially at low pressures, the tests with the largest nozzle (150 µm) have a longer duration of the first phase. This is because with a larger hole, at equal pressures, the fuel output speed is lower, which causes the needle to take longer to fully open the injector.

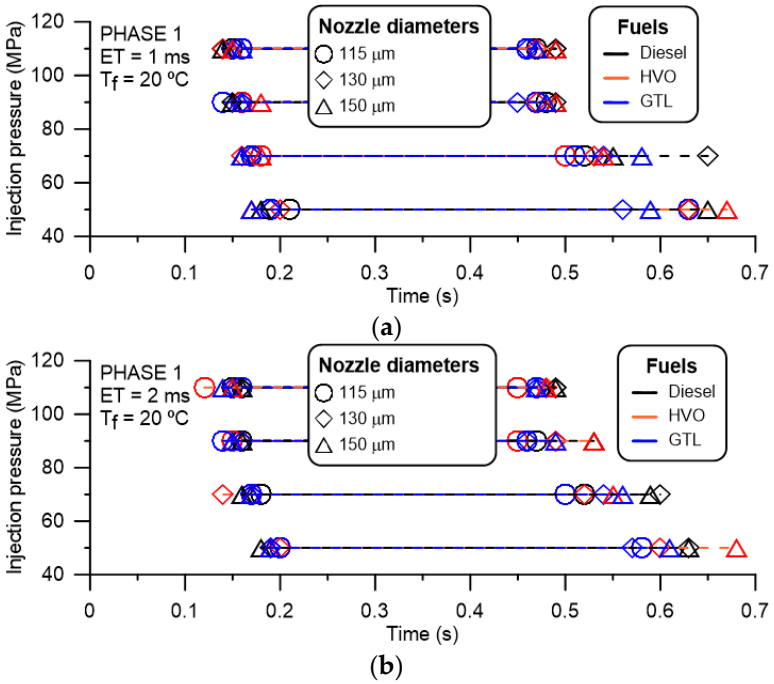

Figure 8. Evolution of the needle lift time (t_{nl}), also denoted as phase 1, with 20 °C (all fuels and all nozzles), (**a**) for 1 ms, and (**b**) for 2 ms.

From the results shown in Tables S2–S4, it can be concluded that:

- In the first phase (needle lift), both the time at which the injection event starts and the time at which it ends decrease with increasing pressure, temperature, and ET, and are more pronounced in HVO.
- In the second phase (holding injection), the start time of this phase evolves, as indicated for the end of the previous phase, and the end time of this phase depends almost entirely on the injection pressure (and, of course, on the ET).
- In the third phase (needle closure), the duration of this phase depends mainly on the injection pressure and ET.

The effect of temperature is more pronounced in the first phase, but in the following phases, the effect is practically null. Something similar occurs with the use of different fuels, the most prominent effect on the duration time of the phases occurs in the first phase.

4. Discussion—Model Validation Results

Comparisons were made between the two curves to graphically present the differences between both the modeled and the experimentally measured rates. In order not to lengthen the text, only part of the results obtained are shown. The three equations developed for the correlations described above are combined to obtain a representation of the injection rate, as shown in Figures 9–11.

4.1. Effect of Nozzle Diameter on the Fuel Injection Rate

Figure 9a–c show the fuel injection rate curves calculated using the three linear models proposed versus experimental fuel injection rate curves obtained from the 70 MPa injection

pressure, ET of 1.5 ms, with the 150, 130, and 115 µm nozzle diameters, and fuel temperature of 40 °C, with diesel fuel.

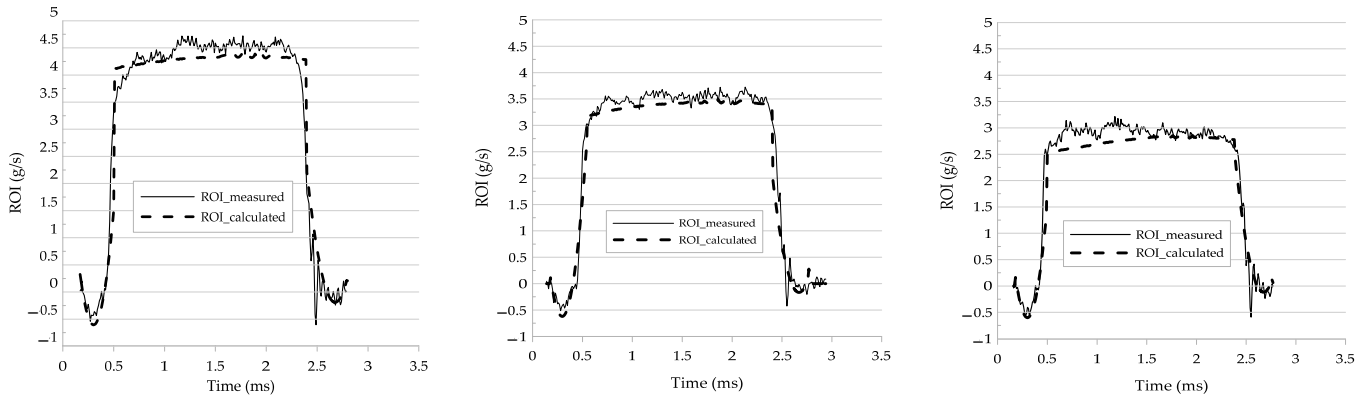

Figure 9. Comparative of measured vs. calculated rate with diesel fuel at 70 MPa injection pressure, ET = 1.5 ms, with nozzle diameters 150 (**a**), 130 (**b**) and 115 (**c**) µm.

The above figures show that the model can fit the experimental results for all three nozzles equally. The effect of the Cd included in Equation (10) is clearly observed. The values of both measured and modeled RoI increase as nozzle diameter increases [57]. The differences between modeled and measured RoI in total mass injected are lower than 15.6% with 115 µm vs. 3.83% with 150 µm.

4.2. Effect of Fuel on the Injection Rate

Equations (11)–(13) can also model the rate with different fuel origins. To demonstrate this capability, Figure 10a–c are shown. In this case, the test conditions used for graphical comparison are: 70 MPa of injection pressure, ET = 2 ms, 130 µm as nozzle diameter, and a fuel temperature of 40 °C. RoI modeled and measured with GtL, HVO, and diesel fuels are shown.

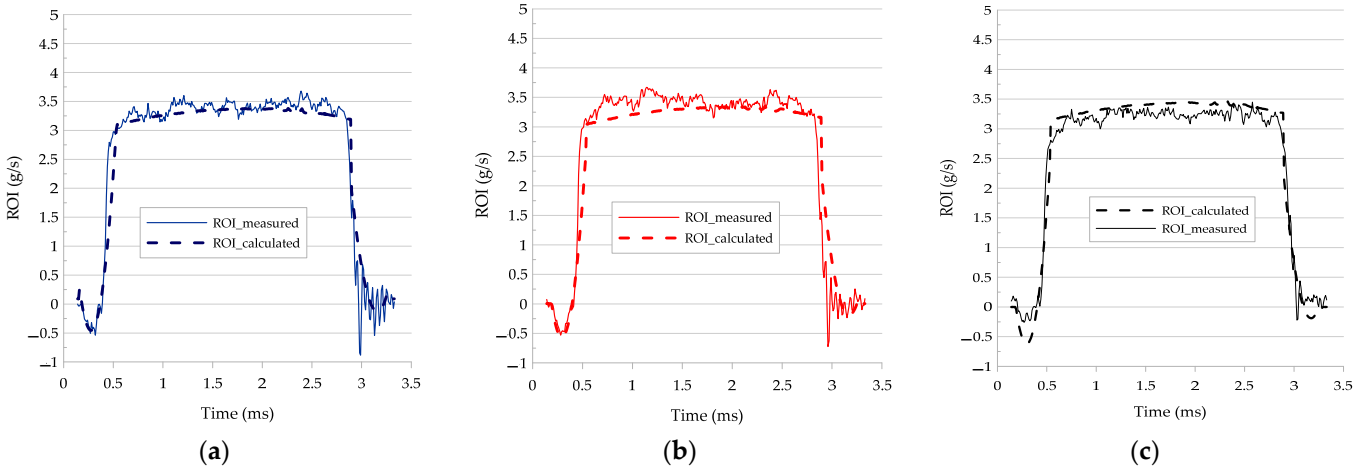

Figure 10. Comparison between measured and calculated fuel injection rates with nozzle diameter 130 µm, ET = 2 ms, and 70 MPa injection pressure, with GtL (**a**), HVO (**b**), and diesel (**c**) fuels.

Figure 10 shows that the model can simulate fuel injection rates with good accuracy. Slight differences in the same order of magnitude are observed with the three fuels studied. In the first and third cases (a and c), the model subestimates the mass flow at 11.15% and 10.87%, respectively, while in case (b), the model subestimates the mass flow at 9.26%.

These results could be justified by the differences in the correlations used for fuel property determination, as explained above in Sections 2.2.2 and 2.2.3.

4.3. Effect of the Energizing Time of the Injector on the Injection Rate

Figure 11a–c, compare both the model and the experimental injection mass flow rate at 50 MPa injection pressure, 115 µm nozzle diameter, fuel temperature of 40 °C, and ET of 2, 1.5, and 1 ms, respectively, with the diesel fuel and fuel temperature of 40 °C.

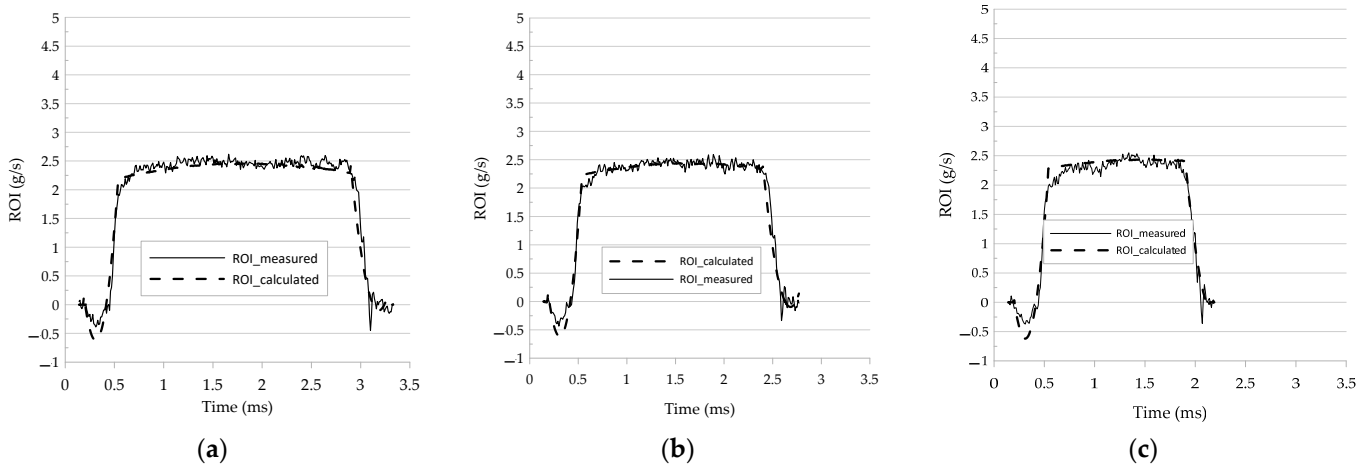

Figure 11. Comparison between both measured and calculated fuel injection rate with diesel fuel, with nozzle diameter 115 µm, 50 MPa injection pressure, 40 °C fuel temperature, and ET of 2 ms (**a**), 1.5 ms (**b**), and 1.0 ms (**c**).

Figure 11 shows that the model can simulate fuel injection rates with better accuracy than the above-presented results. In these cases, the differences are 5.96%, 0.03%, and 3.83% for ET 2.0, 1.5, and 1.0 ms, respectively. The energizing time has been the factor that affects the RoI behavior less.

5. Conclusions

In this study, a 0D model was developed to simulate fuel injection rates from experimental data using mathematical equations based on numerical statistical tools. The study of the experimental tests and the model validation results has allowed us to draw the following conclusions:

- The division of the injection rate signal into three phases (needle lift, holding injection, and needle closure) has allowed the model to better adapt to each phase defined.
- The representativeness study of all variables linked to the experimental trials showed the most important variables affecting the injection rate were fuel properties, nozzle diameter, injection pressure, and energizing time. In addition, it was observed that the most relevant variables varied according to the injection phase. In the first phase (needle lift), injection pressure and test time had a significant influence. In the holding injection phase (second phase), energizing time and hole diameter were the predominant factors. Energizing time and test time had more impact in the needle closure phase (third phase).
- The linear models proposed show high coefficient of determination (R^2) values for the needle lift, holding injection, and needle closure phases, 90.02, 97.24, and 90.45%, respectively. This accuracy analysis methodology provides a solid basis to support the validity and reliability of the results obtained in the study.
- The model can correctly simulate, regardless of hole size. However, it has more difficulty reproducing rates as hole size decreases, an aspect that is probably due to a greater dependence on cavitation in the test.

- Regarding fuels, the model adapts quite well to the use of different fuels, and it has been shown that, even without having the correlations of density and viscosity variation with the exact fuel pressure and temperature (as in the case of HVO fuel), the model can reproduce the injection rate quite well.
- At low pressures, the model starts to have difficulty following the experimental curve. In these situations, the injector needle lift shows more significant oscillation, the discharge process becomes more unstable, and the experimental injection rate curves have less uniformity and stability, which the model cannot reproduce.

In summary, this model can predict rate behavior over different pressure ranges, fuel types, and variations in injection nozzle diameter.

This model proposal can help solve some parts of more complex computational fluid-dynamic predictive models using simple input data from experimental results. Also, this model can be used as input data for thermodynamic predictive models.

Supplementary Materials: The following supporting information can be downloaded at: https://www.mdpi.com/article/10.3390/app14062446/s1, Table S1: Fuel mass injected per stroke (mg/st) in every experimental tested; Table S2: Time values for each phase for nozzle with 115 µm; Table S3: Time values for each phase for nozzle with 130 µm; Table S4: Time values for each phase for nozzle with 150 µm.

Author Contributions: Conceptualization, C.M. and J.A.S.; methodology, V.R.-R.; software, V.R.-R.; validation, C.M. and J.A.S.; formal analysis, V.R.-R.; investigation, V.R.-R.; resources, C.M. and J.A.S.; data curation, V.R.-R.; writing—original draft preparation, V.R.-R.; writing—review and editing, C.M., J.A.S. and O.A.; visualization, V.R.-R.; supervision, O.A.; project administration, O.A.; funding acquisition, O.A. All authors have read and agreed to the published version of the manuscript.

Funding: This research was funded by (i) the government of Castilla-La Mancha community to the project ASUAV, Ref. SBPLY/19/180501/000116, and (ii) Contribution from the national project (PID2020-118387RB-C32).

Institutional Review Board Statement: Not applicable.

Informed Consent Statement: Not applicable.

Data Availability Statement: The original contributions presented in the study are included in the article, further inquiries can be directed to the corresponding author.

Acknowledgments: Authors want to thank the Universidad Politécnica Salesiana to Quito to the Research Pre-doctoral Grant to Vicente Rojas.

Conflicts of Interest: The authors declare no conflicts of interest.

References

1. Tennison, P.; Reitz, R. An Experimental Investigation of the Effects of Common-Rail Injection System Parameters on Emissions and Performance in a High-Speed Direct-Injection Diesel Engine. *ASME J. Eng. Gas Turbines Power* **2001**, *123*, 167–174. [CrossRef]
2. Agarwal, A.K.; Srivastava, D.K.; Dhar, A.; Maurya, R.K.; Shukla, P.C.; Singh, A.P. Effect of fuel injection timing and pressure on combustion, emissions and performance characteristics of a single cylinder diesel engine. *Fuel* **2013**, *111*, 374–383. [CrossRef]
3. Mohamed Shameer, P.; Ramesh, K.; Sakthivel, R.; Purnachandran, R. Effects of fuel injection parameters on emission characteristics of diesel engines operating on various biodiesel: A review. *Renew. Sustain. Energy Rev.* **2017**, *67*, 1267–1281. [CrossRef]
4. Skrzek, T.; Jarzyński, G. Research on the impact of diesel injection parameters on particulate matters emission in a dual-fuel supercharged engine fueled with natural gas. *AUTOBUSY* **2018**, *19*, 233–237. [CrossRef]
5. Lee, C.; Park, S. An experimental and numerical study on fuel atomization characteristics of high-pressure diesel injection sprays. *Fuel* **2002**, *81*, 2417–2423. [CrossRef]
6. Rua-Mojica, L.F.; Rubio-Gómez, G.; Corral-Gómez, L.; Martínez-Martínez, S.; Sánchez-Cruz, F.A.; Armas-Vergel, O. Numerical and experimental study of atomization characteristics on injection sprays for alternative and diesel fuels. In Proceedings of the Symposium on Renewable Energies and Thermal Sciences, Salamanca, Guanajuato, Mexico, 15–17 March 2017; Available online: https://www.grupogpem.com/publications/congress-contributions/ (accessed on 15 January 2024).
7. Markov, V.; Sa, B.; Devyanin, S.; Grekhov, L.; Neverov, V.; Zhao, J. Numerical analysis of injection and spray characteristics of diesel fuel and rapeseed oil in a diesel engine. *Case Stud. Therm. Eng.* **2022**, *35*, 102129. [CrossRef]
8. Yu, J.; Feng, R.; Wang, S.; Deng, B. The influence of particle oxidation catalyst (POC) mode on emissions reduction of a turbo-charging non-road diesel under wide operating conditions. *Therm. Sci. Eng. Prog.* **2024**, *47*, 102357. [CrossRef]

9. Deng, B.; Chen, Z.; Sun, C.; Zhang, S.; Yu, W.; Huang, M.; Hou, K.; Ran, J.; Zhou, L.; Chen, C.; et al. Key design and layout factors influencing performance of three-way catalytic converters: Experimental and semidecoupled numerical study under real-life driving conditions. *J. Clean. Prod.* **2023**, *425*, 138993. [CrossRef]
10. Da Costa, R.B.R.; Coronado, C.J.R.; Hernández, J.J.; Malaquias, A.C.T.; Flores, L.F.V.; De Carvalho, J.A. Experimental assessment of power generation using a compression ignition engine fueled by farnesane—A renewable diesel from sugarcane. *Energy* **2021**, *233*, 121187. [CrossRef]
11. Soto, F.; Marques, G.; Torres-Jiménez, E.; Vieira, B.; Lacerda, A.; Armas, O.; Guerrero-Villar, F. A comparative study of performance and regulated emissions in a medium-duty diesel engine fueled with sugarcane diesel-farnesane and sugarcane biodiesel-LS9. *Energy* **2019**, *176*, 392–409. [CrossRef]
12. Wu, S.; Kang, D.; Xiao, R.; Boehman, A.L. Autoignition characteristics of bio-based fuels, farnesane and TPGME, in comparison with fuels of similar cetane rating. *Proc. Combust. Inst.* **2021**, *38*, 5585–5595. [CrossRef]
13. Da Costa, R.B.R.; Roque, L.F.A.; De Souza, T.A.Z.; Coronado, C.J.R.; Pinto, G.M.; Cintra, A.J.A.; Raats, O.O.; Oliveira, B.M.; Frez, G.V.; Da Silva, M.H. Experimental assessment of renewable diesel fuels (HVO/Farnesane) and bioethanol on dual-fuel mode. *Energy Convers. Manag.* **2022**, *258*, 115554. [CrossRef]
14. Mata, C.; Cárdenas, D.; Esarte, C.; Soriano, J.A.; Gómez, A.; Fernández-Yáñez, P.; García-Contreras, R.; Sánchez, L.; Nogueira, J.I.; Armas, O. Performance and regulated emissions from a Euro VI-D hybrid bus tested with fossil and renewable (hydrotreated vegetable oil) diesel fuels under urban driving in Bilbao city, Spain. *J. Clean. Prod.* **2022**, *383*, 135472. [CrossRef]
15. Payri, R.; Salvador, F.J.; Martí-Aldaraví, P.; Martínez-López, J. Using one-dimensional modeling to analyse the influence of the use of biodiesels on the dynamic behavior of solenoid-operated injectors in common rail systems: Detailed injection system model. *Energy Convers. Manag.* **2011**, *54*, 90–99. [CrossRef]
16. Boudy, F.; Seers, P. Impact of physical properties of biodiesel on the injection process in a common-rail direct injection system. *Energy Convers. Manag.* **2009**, *50*, 2905–2912. [CrossRef]
17. Selvaraj, M.; Subbiah, G. The influence of injection parameters on the performance and emission characteristics of a DI diesel engine using biofuel-blended-pure diesel fuel. *Ambient. Energy* **2018**, *40*, 800–803. [CrossRef]
18. Yehliu, K.; Boehman, A.L.; Armas, O. Emissions from different alternative diesel fuels operating with single and split fuel injection. *Fuel* **2009**, *89*, 423–437. [CrossRef]
19. Dimitriadis, A.; Seljak, T.; Vihar, R.; Baškovič, U.Ž.; Dimaratos, A.; Bezergianni, S.; Samaras, Z.; Katrašnik, T. Improving PM-NOx trade-off with paraffinic fuels: A study towards diesel engine optimization with HVO. *Fuel* **2019**, *265*, 116921. [CrossRef]
20. Preuss, J.; Munch, K.; Denbratt, I. *Effect of Injection Strategy and EGR on Particle Emissions from a CI Engine Fueled with an Oxygenated Fuel Blend and HVO*; SAE Technical Paper No. 2021-01-0560; SAE: Warrendale, PA, USA, 2021. [CrossRef]
21. Carlucci, P.; Ficarella, A.; Laforgia, D. Effects on combustion and emissions of early and pilot fuel injections in diesel engines. *Int. J. Engine Res.* **2005**, *6*, 43–60. [CrossRef]
22. Luján, J.M.; Tormos, B.; Salvador, F.J.; Gargar, K. Comparative analysis of a DI diesel engine fuelled with biodiesel blends during the European MVEG-A cycle: Preliminary study I. *Biomass Bioenergy* **2009**, *33*, 941–947. [CrossRef]
23. Dernotte, J.; Hespel, C.; Foucher, F.; Houillé, S.; Mounaïm-Rousselle, C. Influence of physical fuel properties on the injection rate in a Diesel injector. *Fuel* **2011**, *96*, 153–160. [CrossRef]
24. Salvador, F.J.; Gimeno, J.; La Morena, J.; Carreres, M. Using one-dimensional modeling to analyze the influence of the use of biodiesels on the dynamic behavior of solenoid-operated injectors in common rail systems: Results of the simulations and discussion. *Energy Convers. Manag.* **2011**, *54*, 122–132. [CrossRef]
25. Allocca, L.; Montanaro, A.; Cipolla, G.; Vassallo, A. *Spatial-Temporal Characterization of Alternative Fuel Sprays from a Second-Generation Common-Rail Fuel Injection System for Euro4 Passenger Car Application*; SAE Technical Paper no. 2009-01-1856; SAE: Warrendale, PA, USA, 2009. [CrossRef]
26. Han, D.; Wang, C.; Duan, Y.; Tian, Z.; Huang, Z. An experimental study of injection and spray characteristics of diesel and gasoline blends on a common rail injection system. *Energy* **2014**, *75*, 513–519. [CrossRef]
27. Payri, R.; Bracho, G.; Soriano, J.A.; Fernández-Yáñez, P.; Armas, O. Nozzle rate of injection estimation from hole to hole momentum flux data with different fossil and renewable fuels. *Fuel* **2020**, *279*, 118404. [CrossRef]
28. Rojas-Reinoso, V.; Duque-Escobar, S.; Guapulema-Guapulema, C.; Soriano, J.A. Study of the Variation of Fuel Pressure to Improve Spraying and the Range of the Injection Jet. *Energies* **2023**, *16*, 5472. [CrossRef]
29. Mata, C.; Rojas-Reinoso, V.; Soriano, J.A. Experimental determination and modelling of fuel rate of injection: A review. *Fuel* **2023**, *343*, 127895. [CrossRef]
30. Payri, R.; Lopez, J.; Salvador, F.J.; Martí-Aldaraví, P. Development of a Methodology to Learn the Characteristics and Performances of Common Rail Injection Systems Based on Simulations with AMESim. *Int. J. Eng. Educ.* **2013**, *29*, 533–547.
31. Soriano, J.A.; Mata, C.; Armas, O.; Ávila, C. A zero-dimensional model to simulate injection rate from first generation common rail diesel injectors under thermodynamic diagnosis. *Energy* **2018**, *158*, 845–858. [CrossRef]
32. Postrioti, L.; Malaguti, S.; Bosi, M.; Buitoni, G.; Piccinini, S.; Bagli, G. Experimental and numerical characterization of a direct solenoid actuation injector for Diesel engine applications. *Fuel* **2013**, *118*, 316–328. [CrossRef]
33. Ferrari, A.; Paolicelli, F. An indirect method for the real-time evaluation of the fuel mass injected in small injections in Common Rail diesel engines. *Fuel* **2016**, *191*, 322–329. [CrossRef]

34. Salvador, F.J.; Gimeno, J.; Martín, J.; Carreres, M. Thermal effects on the diesel injector performance through adiabatic 1D modelling. Part I: Model description and assessment of the adiabatic flow hypothesis. *Fuel* **2019**, *260*, 116348. [CrossRef]
35. Vass, S.; Németh, H. Sensitivity analysis of instantaneous fuel injection rate determination for detailed Diesel combustion models. *Period. Polytech. Transp. Eng.* **2013**, *41*, 77. [CrossRef]
36. Payri, R.; Salvador, F.J.; Gimeno, J.; De la Morena, J. Influence of injector technology on injection and combustion development—Part 1: Hydraulic characterization. *Appl. Energy* **2010**, *88*, 1068–1074. [CrossRef]
37. Herfatmanesh, M.R.; Lu, P.; Attar, M.A.; Zhao, H. Experimental investigation into the effects of two-stage injection on fuel injection quantity, combustion and emissions in a high-speed optical common rail diesel engine. *Fuel* **2013**, *109*, 137–147. [CrossRef]
38. Payri, R.; Molina, S.; Salvador, F.J.; Gimeno, J. A study of the relation between nozzle geometry, internal flow and sprays characteristics in diesel fuel injection systems. *KSME Int. J.* **2004**, *18*, 1222–1235. [CrossRef]
39. Kastengren, A.; Ilavsky, J.; Viera, J.P.; Payri, R.; Duke, D.J.; Swantek, A.; Zak Tilocco, F.; Sovis, N.; Powell, C.F. Measurements of droplet size in shear-driven atomization using ultra-small angle X-ray scattering. *Int. J. Multiph. Flow* **2017**, *92*, 131–139. [CrossRef]
40. Kevorkijan, L.; Palomar-Torres, A.; Torres-Jiménez, E.; Mata, C.; Biluš, I.; Lešnik, L. Obtaining the Synthetic Fuels from Waste Plastic and Their Effect on Cavitation Formation in a Common-Rail Diesel Injector. *Sustainability* **2023**, *15*, 15380. [CrossRef]
41. Lešnik, L.; Palomar-Torres, A.; Torres-Jiménez, E.; Mata, C.; Volmajer Valh, J.; Kevorkijan, L.; Biluš, I. The effect of HDPE and LDPE pyrolytic oils on cavitation formation in a common-rail diesel injector. *Fuel* **2022**, *330*, 125581. [CrossRef]
42. Payri, R.; Gimeno, J.; Novella, R.; Bracho, G. On the rate of injection modeling applied to direct injection compression ignition engines. *Int. J. Engine Res.* **2016**, *17*, 1015–1030. [CrossRef]
43. Xu, L.; Bai, X.-S.; Jia, M.; Qian, Y.; Qiao, X.; Lu, X. Experimental and modeling study of liquid fuel injection and combustion in diesel engines with a common rail injection system. *Appl. Energy* **2018**, *230*, 287–304. [CrossRef]
44. Agarwal, A.K.; Dhar, A.; Gupta, J.G.; Kim, W.I.; Lee, C.S.; Park, S. Effect of fuel injection pressure and injection timing on spray characteristics and particulate size–number distribution in a biodiesel fuelled common rail direct injection diesel engine. *Appl. Energy* **2014**, *130*, 212–221. [CrossRef]
45. Seykens, X.; Somers, L.M.T.; Baert, R. Modeling of common rail fuel injection system and influence of fluid properties on injection process. In Proceedings of the International Conference on Vehicle Alternative Fuel Systems and Environmental Protection, Dublin, Ireland, 6–7 July 2004; Olabi, A.G., Ed.; Dublin City University: Dublin, Ireland, 2004; pp. 72–77.
46. Li, X.; Li, D.; Pei, Y.; Peng, Z. Optimising microscopic spray characteristics and particle emissions in a dual-injection spark ignition (SI) engine by changing GDI injection pressure. *Int. J. Engine Res.* **2022**, 14680874221082793. [CrossRef]
47. Gao, Z.; Li, G.; Xu, C.; Li, H.; Wang, M. A calculation method and experiment study of high-pressure common rail injection rate with solenoid injectors. *Sci. Prog.* **2021**, *104*, 368504211026157. [CrossRef]
48. Perini, F.; Busch, S.; Reitz, R.D. A phenomenological rate of injection model for predicting fuel injection with application to mixture formation in light-duty diesel engines. *Proc. Inst. Mech. Eng. Part. D* **2020**, *234*, 1826–1839. [CrossRef]
49. Bosch, W. *The Fuel Rate Indicator: A New Measuring Instrument for Display of the Characteristics of Individual Injection*; SAE Technical Paper; SAE: Warrendale, PA, USA, 1966; p. 660749. [CrossRef]
50. Armas, O.; Martínez-Martínez, S.; Mata, C.; Pacheco, C. Alternative method for bulk modulus estimation of Diesel fuels. *Fuel* **2016**, *167*, 199e207. [CrossRef]
51. Payri, R.; Salvador, F.J.; Gimeno, J.; Bracho, G. The effect of temperature and pressure on thermodynamic properties of diesel and biodiesel fuels. *Fuel* **2010**, *90*, 1172–1180. [CrossRef]
52. Outcalt, S.L. Compressed-liquid density measurements of three alternative turbine fuels. *Fuel* **2014**, *124*, 1–6. [CrossRef]
53. Rackett, H.G. Equation of State for Saturated Liquids. *J. Chem. Eng. Data* **1970**, *15*, 514–517. [CrossRef]
54. Dymond, J.H.; Malhotra, R. The Tait equation: 100 years on. *Int. J. Thermophys.* **1988**, *9*, 941–951. [CrossRef]
55. Kousel, B. How pressure affects liquid viscosity. *Hydrocarb. Process Pet.* **1965**, *44*, 120–130.
56. Lešnik, L.; Kegl, B.; Torres-Jiménez, E.; Cruz-Peragón, F.; Mata, C.; Biluš, I. Effect of the In-Cylinder Back Pressure on the Injection Process and Fuel Flow Characteristics in a Common-Rail Diesel Injector Using GTL Fuel. *Energies* **2021**, *14*, 452. [CrossRef]
57. Payri, R.; Hardy, G.; Gimeno, J.; Bautista, A. Analysis of counterbore effect in five diesel common rail injectors. *Exp. Therm. Fluid Sci.* **2019**, *107*, 69–78. [CrossRef]